Original article
DOI: https://doi.org/10.18721/JPM.18106

NUMERICAL SIMULATION OF UNDER-ICE RADIATIVELY DRIVEN CONVECTION IN LAKES WITH DIFFERENT WATER TRANSPARENCY

S. I. Smirnov[1]✉, *A. A. Smirnovsky*[2], *S. R. Bogdanov*[1], *G. E. Zdorovennova*[1], *T. V. Efremova*[1], *N. I. Palshin*[1], *R. E. Zdorovennov*[1]

[1] Northern Water Problems Institute of Karelian Research Centre of RAS, Petrozavodsk, Russia;

[2] Peter the Great St. Petersburg Polytechnic University, St. Petersburg, Russia

✉ sergeysmirnov92@mail.ru

Abstract. In the paper, the results of eddy-resolving numerical simulation of convection generated by inhomogeneous heating of water column by solar radiation in an ice-covered shallow lake (the factor of wind impact on the water surface is excluded). The calculations have been performed using the Implicit LES method for different values of the extinction coefficient, which defines the degree of attenuation of solar radiation in the water column. An analysis of the three-dimensional flow structure, the time evolution of temperature and velocity pulsations was carried out, and the increments of the lower boundary and the temperature of the convective mixed layer were calculated depending on the incoming heat. The results obtained shed light upon the nature of the processes occurring in the type of lakes under consideration, in particular, to identify the influence of water transparency on the convective mixing process.

Keywords: radiatively-driven under-ice convection, water transparency, turbulent velocity pulsations, Implicit LES

Funding: The reported study was carried out within the framework of the State Assignment of Northern Water Problems Institute of Karelian Research Centre of RAS (FMEN 2021-0019).

Citation: Smirnov S. I., Smirnovsky A. A., Bogdanov S. R., Zdorovennova G. E., Efremova T. V., Palshin N. I., Zdorovennov R. E., Numerical simulation of under-ice radiatively-driven convection in lakes with different water transparency, St. Petersburg State Polytechnical University Journal. Physics and Mathematics. 18 (1) (2025) 69–86. DOI: https://doi.org/10.18721/JPM.18106

Научная статья
УДК 556.555.4/.5; 556.556
DOI: https://doi.org/10.18721/JPM.18106

ЧИСЛЕННОЕ МОДЕЛИРОВАНИЕ ПОДЛЕДНОЙ РАДИАЦИОННО-ГЕНЕРИРУЕМОЙ КОНВЕКЦИИ В ОЗЕРАХ С РАЗНОЙ ПРОЗРАЧНОСТЬЮ ВОДЫ

С. И. Смирнов[1]✉, А. А. Смирновский[2], С. Р. Богданов[1], Г. Э. Здоровеннова[1], Т. В. Ефремова[1], Н. И. Пальшин[1], Р. Э. Здоровеннов[1]

[1] Институт водных проблем Севера Карельского научного центра РАН, г. Петрозаводск, Россия;

[2] Санкт-Петербургский политехнический университет Петра Великого, Санкт-Петербург, Россия

✉ sergeysmirnov92@mail.ru

Аннотация. Представлены результаты вихреразрешающего численного моделирования конвекции, возникающей в результате неоднородного прогрева водной толщи мелководного озера, покрытого льдом (т. е. без воздействия ветра на водную поверхность). Расчеты проводились с использованием метода Implicit LES при различных значениях коэффициентов экстинкции, характеризующих поглощение солнечной радиации толщей воды. Проведен анализ трехмерной структуры течения, временной эволюции температуры и пульсаций скорости, а также рассчитаны приращения нижней границы и температуры конвективно-перемешанного слоя в зависимости от поступающего в систему тепла. Полученные результаты позволяют уточнить особенности термического режима рассмотренного типа озер в период формирования подледного конвективно-перемешанного слоя, в частности — выявить влияние прозрачности воды на процесс перемешивания.

Ключевые слова: радиационно-генерируемая подледная конвекция, прозрачность воды, турбулентные пульсации скорости, метод крупных вихрей

Финансирование: Исследование выполнено в рамках государственного задания Института водных проблем Севера Карельского научного центра РАН (FMEN 2021-0019).

Ссылка для цитирования: Смирнов С. И., Смирновский А. А., Богданов С. Р., Здоровеннова Г. Э., Ефремова Т. В., Пальшин Н. И., Здоровеннов Р. Э. Численное моделирование подледной радиационно-генерируемой конвекции в озерах с разной прозрачностью воды // Научно-технические ведомости СПбГПУ. Физико-математические науки. 2025. Т. 18. № 1. С. 69–86. DOI: https://doi.org/10.18721/JPM.18106

Introduction

Radiatively driven convection (RDC) plays a major role in mixing of water masses in lakes in the late winter and early spring, when ice-covered lakes are exposed to heating by solar radiation, while there is no direct effect of wind on the water surface. The driving force of this type of convection is inhomogeneous heating of the water layers by solar rays penetrating under the ice, in the temperature range from 0 °C to about 4 °C (the temperature of the maximum density of freshwater T_{md}) [1–3]. RDC can continue even after the ice melts if the water temperature is below T_{md}. This process stops when the surface layer of the lake warms up above T_{md}.

RDC plays an important role in the functioning of lake ecosystems, as convective flows transport nutrients to the photic zone and redistribute algae cells along the water column, thus contributing to the development of the planktonic community and the metabolism dynamics [4–6].

An overview of theoretical and experimental research into RDC is presented in [7]. The main theoretical and model ideas of the RDC are described in [8], analyzing stability modes and stratification dynamics. Various convection modes, including RDC in ice-covered lakes are reviewed in [3].

RDC during the ice age has been studied for many years in the shallow Lake Vendyurskoye (located in the territory of the Petrovskoye rural settlement of the Kondopozhsky District of Republic of Karelia, Russia) based on measurements of solar radiation fluxes, water temperature at different depths of the water column and velocity components [2, 7]. High-frequency measurements of water temperature and flow velocity over several days allowed to trace the diurnal evolution of buoyancy-driven flow due to variation in the solar flux and the dissipation rate of turbulence kinetic energy in a convective mixed layer (CML).

Large Eddy Simulation (LES) is widely used to study flows in natural waters [9–11]. If the so-called Implicit LES approach is used, the effect of turbulent flow on subgrid scales is simulated by the dissipative properties of the corresponding numerical scheme. This approach has proved advantageous for solving problems of natural-convection flows (see, for example, [12–14]). Mironov et al. performed numerical simulations based on the LES approach for idealized conditions of RDC in a shallow lake; overturning plumes were observed in the convective layer, helping describe the entrainment processes of the underlying water layers [9]. Recent RDC simulations [15–17] also show good agreement between the numerical results and field observations.

An important parameter governing the evolution of convective mixing in an ice-covered lake is the degree of water transparency. One-dimensional models used for lakes of the boreal [18] and arid [19] zones for the open-water period point to enhanced heat accumulation in the surface layer at high values of the extinction coefficient. It was observed that when the water is more turbid (and, accordingly, the extinction coefficient is higher), and the solar fluxes entering the surface of the water body are equal with different water transparency, the mixed surface layer is thinner, and the average temperature of the water column is lower than in the case of clearer waters (lower extinction coefficients). The heat distribution over a water column was studied for an ice-covered lake within the framework of a one-dimensional model as a function of the extinction coefficient of water, finding that the higher this coefficient, the greater the proportion of heat absorbed by the surface layer and the less heat reaches the underlying layers [20].

The goal of this study is to evaluate the effect from the degree of transparency of water on the structure of a convective mixed layer during radiatively-driven convection. The evaluation is based on eddy-resolving approaches.

This paper presents the results of the initial stages of CML evolution for three cases of water transparency.

Problem statement and computational aspects

The problem statement is similar to that described in previous papers [15–17]. The computational domain is a rectangular parallelepiped with dimensions $L \times L \times H$, where L is the size of the domain in the horizontal directions x and y ($L = 9.6$ m), H is the height of the computational domain ($H = 6.4$ m) (Fig. 1).

Previous studies found that the size of the computational domain (9.6 × 9.6 × 6.4 m) is sufficient for conducting numerical simulation of RDC in the under-ice layer of a small lake at the early stages of CML formation and development. A constant temperature of 0 °C and the no-slip conditions for the velocity were imposed at the upper boundary of the computational domain simulating the lower surface of the ice. It was assumed that there was no flow during the entire period under consideration near the lower boundary of the computational domain simulating the conditional bottom of the lake; the conditions imposed for this surface were no-slip and constant heat flux corresponding to a temperature gradient of 0.4 °C/m, which is typical for the bottom layers of small shallow lakes; in particular, this corresponds to field observations in Lake Vendyurskoye [21]. Periodicity conditions were imposed in the horizontal directions.

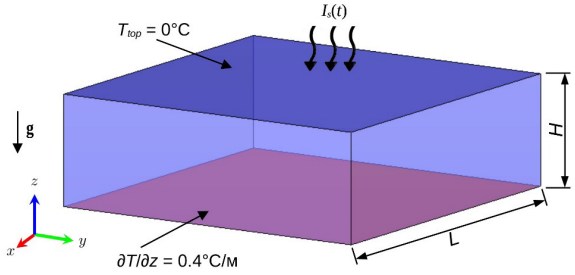

Fig. 1. Geometry of computational domain and thermal boundary conditions, $I_s(t)$ is the kinematic flux of solar heat

A linear temperature profile corresponding to the boundary conditions, and a zero velocity field were given as the initial fields were. This formulation of the problem is idealized: in reality, the depth distribution of temperature may vary at the beginning of the RDC period for different lakes and the temperature increase along the depth may differ from linear. Note that time zero in the simulations corresponded to 6 a.m., i.e., the time when radiation started to penetrate the under-ice layer of water (see Fig. 2 in [5]).

Turbulent heat and mass transfer is calculated based on a system of equations including the continuity equation (1), Navier–Stokes equations (2) written taking into account the buoyancy effects in a gravitational field in the Boussinesq approximation, and energy equation (3) taking into account the volumetric heat generation due to absorption of solar radiation:

$$\nabla \cdot \mathbf{V} = 0, \tag{1}$$

$$\frac{\partial \mathbf{V}}{\partial t} + (\mathbf{V} \cdot \nabla)\mathbf{V} = -\frac{1}{\rho}\nabla p - \beta(T - T_0)\mathbf{g} + \nu\nabla^2\mathbf{V}, \tag{2}$$

$$\frac{\partial T}{\partial t} + (\mathbf{V} \cdot \nabla)T = \alpha\nabla^2 T + \frac{\partial I}{\partial h}, \tag{3}$$

where $\mathbf{V}$, m/s, is the flow velocity vector; ρ, kg/m^3, is the density; p, Pa, is the pressure; ν, m^2/s, is the kinematic viscosity; α, m^2/s, is the thermal conductivity; β, K^{-1}, is the coefficient of thermal expansion; T_0 and T, °C, are the temperature under hydrostatic equilibrium and instantaneous temperature; I, K·m/s, is the solar radiation flux; h, m, is the depth of the lake (measured from the lower surface of the ice and directed opposite to the z axis); $\mathbf{g}$, m/s^2, is the gravitational acceleration; t, s, *is* the time.

The coefficient β was calculated based from the approximation of the dependence of freshwater density on temperature:

$$\beta = b_1 \cdot (T - T_{md}), \tag{4}$$

where $b_1 = 1.65 \cdot 10^{-5}$ K^{-2}; T_{md} is the temperature of maximum freshwater density, as mentioned above ($T_{md} = 3.84$ °C was assumed in the calculations).

This dependence holds true in the temperature range $0-T_{md}$ (°C). The remaining physical parameters were constants and had corresponding values for clear water at a temperature of 2 °C.

The right-hand side of energy equation (3) includes a volumetric heat source $\partial I/\partial h$, simulating the absorbed solar radiation in the simulations. The two-parameter law of heat flux attenuation over depth h was used:

$$I(h, t) = I_s(t) \cdot [a_1 \exp(-\gamma_1 h) + a_2 \exp(-\gamma_2 h)], \tag{5}$$

where $I_s(t)$ is the kinematic heat flux at the lower boundary of the ice, i.e., the heat flux divided by density and specific heat. The parameters a_1 and a_2 were taken to be equal: $a_1 = a_2 = 0.5$.

In this paper, we consider three simulation scenarios (V1–V3), which differ only in the values of extinction coefficients γ (Fig. 2).

V1: $\gamma_1 = 2.7$ m^{-1}, $\gamma_2 = 0.7$ m^{-1} (initial case corresponding to field observations in Lake Vendyurskoe);

V2: $\gamma_1 = \gamma_2 = 0.7$ m^{-1} (case of clear water);

V3: $\gamma_1 = \gamma_2 = 2.7$ m^{-1} (case of turbid water).

A higher value of the extinction coefficient characterizes the attenuation of radiation in the upper layer, where the long-wavelength region of the spectrum is absorbed, while a lower value characterizes the transparency of the underlying water column.

The computational results for the initial case V1 were published earlier in [15, 16]. The lower values of the extinction coefficient (V2) correspond to lakes with a high degree of transparency, where the incident radiation penerates deep into the water column. The case V3 corresponding to higher values of the parameter γ is typical for lakes with low water transparency.

The heat flux $I_s(t)$ was described by the approximation of field observation data obtained during the RDC studies in Lake Vendyurskoye in the spring of 2020:

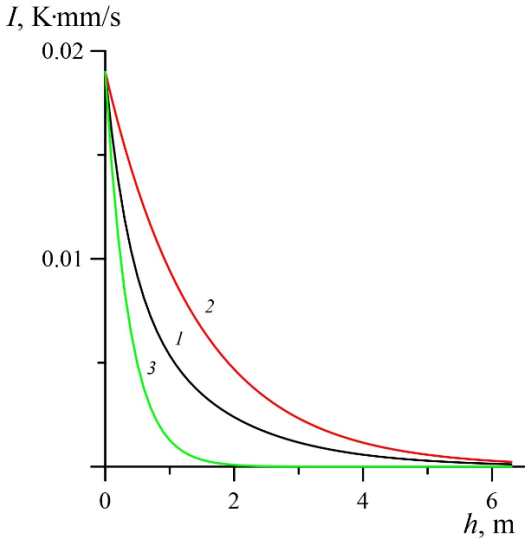

Fig. 2. Dependences of radiation flux on lake depth (h = 0 is the lower surface of the ice) for cases V1–V3 (curves *1*, *2*, *3*, respectively). V1 are the extinction coefficients corresponding to field observations; V2, V3 correspond to clear (V2) or turbid (V3) water

$$I_s(t) = I_0 \cdot \max\{\sin(2\pi t/T^*), 0\}, \qquad (6)$$

where T^* is the time period (T^* = 24 h); $I_0 = 1.9 \cdot 10^{-5}$ K·m/s (see Fig. 2 in [15]).

The simulations were performed using the finite-volume program code SINF/Flag-S, developed at Peter the Great St. Petersburg Polytechnic University [13, 22, 23]. The SIMPLEC algorithm with second-order accuracy was used for time advancement. Spatial approximation of convective terms was carried out by the QUICK (Quadratic Upstream Interpretation for Convective Kinematics) scheme. Diffusion terms were approximated by a central-difference scheme with second-order accuracy. The Implicit LES (ILES) method was used as a vortex-resolving approach.

The computational mesh used consisted of hexagonal elements. The number of elements was 27 million. The time step was chosen to be 2.5 s. The computational details and the estimation of Kolmogorov scales in CML are described in more detail in [15, 16].

Computational results and discussion

A detailed description of the evolution and structure of the flow (for the initial case V1) was presented earlier in [15, 16]. Here we briefly describe only the main results obtained.

The presented distribution of the evolution of water temperature for case V1 (Fig. 3,*a*) is in good agreement with the corresponding variations in the temperature fields of water, obtained in observations conducted with a similar radiation flux at the lower boundary of the ice. Evidently, the upper layers of water warm up first, and the CML gradually thickens, entraining the lower layers. Simulations performed with other values of the extinction coefficient show similar dynamics. Depending on the value of the parameter γ, either weak warming of the upper layers and stronger warming of the lower ones is observed, compared with the initial case V1 (case V2, Fig. 3,*b*), or, vice versa, rapid warming of the upper layers and slow increase in temperature in the lower layers (V3, Fig. 3,*c*). The main high-frequency temperature fluctuations (see Fig. 3), concentrated at the interface between the CML and the boundary subglacial layer during daytime (depth h = 0.1–0.2 m).

Let us focus more closely on the distribution of temperature averaged in horizontal planes over the depth of the layer for three cases (Figs. 4 and 5). First, let us analyze the process of CML formation, occurring at different times for different cases. The fastest formation of CML, occurring between 4 and 5 hours after the start of heating, was observed for the case V3 with the highest value of γ (see Fig. 4,*a*). The 'collapse' of the unstable temperature profile occurs in several stages (red curves in Fig. 4,*a*). The temperature profile inside the CML takes approximately 5 hours to fully form after the start of heating (simulations), which corresponds to 11 in the morning. A similar temperature evolution occurs in the first hours for the initial case (see Fig. 4,*b*). Due to slower warming of the upper layers, the formation of CML was observed later, between 6 and 7 hours after the start of the simulation. The picture of temperature evolution during these hours (red curves in Fig. 4,*b*) is similar to that for case V3. The situation is noticeably different for V2 (see Fig. 4,*c*). While CML formation for V1 and V3 occurred on the first day with a difference of about two hours, the process of temperature profile transformation for V2 was completed only on the third day (red curves in Fig. 4,*c*).

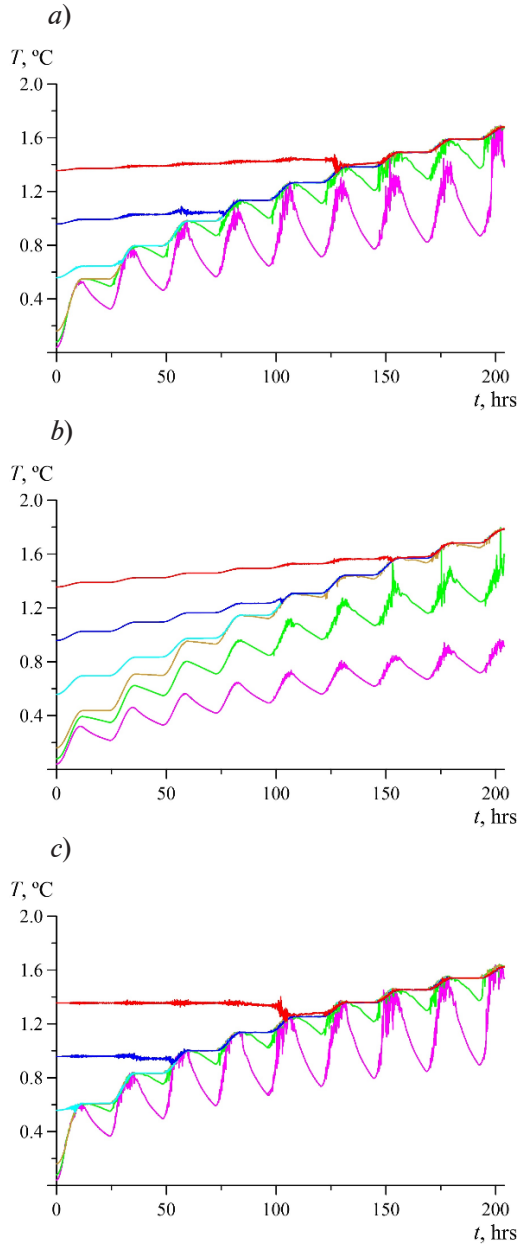

Fig. 3. Temperature evolution for cases V1(*a*), V2(*b*) and V3(*c*) over nine days at different depths *h*, m: 0.1 (purple curve), 0.2 (green), 0.4 (brown), 1.4 (blue), 2.4 (blue), 3.4 (red color)

This result is explained by the fact that intensive warming of the upper layers and weak warming of the lower layers occurs in the case of low transparency of the lake: a thin layer quickly forms in the upper part of the water column at the heating stage, such that its temperature is higher (and, consequently, the density is greater) than that of the underlying layers. As the kinematic flux simulating the radiatively driven heating of an ice-covered lake during daytime increases over time, a region forms in the upper part of the temperature profile where the temperature (density) values at a certain time become higher than in the adjacent underlying layer, the temperature difference quickly reaches a critical value at which a 'collapse' occurs and convective motion evolves. The temperature continues to increase in the upper part of the water column, while 'collapses' continue as well, which gradually leads to the formation of a convective mixed layer. During the daytime, a series of 'collapses' continuously occur, preserving the CML. At night, when the heat flux at the upper boundary of the computational domain disappears, the process of 'collapses' stops. The boundaries of the CML gradually blur during the nighttime, and a temperature gradient appears by the end of the night in the bulk of the mixed layer, but it is noticeably smaller than in the underlying stratified layer. In the case V2 (greater transparency of the lake), heat is distributed more evenly over the water column, which leads to a much later 'collapse' of the temperature profile and a delay in the formation of CML. The process of profile 'collapse (i.e., the development of convective flow after the unstable stratification) takes about one hour in all cases considered. Nevertheless, such a dramatic difference in the time of profile transformation for different cases suggests a significant nonlinearity and complexity of flow evolution in the under-ice layer.

Let us consider the evolution of the averaged temperature profiles of the formed CML for various cases. Fig. 5 shows the temperature distributions over depth at different points in time, starting on the third day, when the CML already developed for all cases. The CML temperatures in the middle of the third day are close to each other, with $T_{V2} < T_{V1} < T_{V3}$. However, their order changed by the 9th day: $T_{V2} > T_{V1} > T_{V3}$. Therefore, the temperature growth rate in CML is the highest for V2 for the time period under consideration.

Thus, in the case of a fairly well-developed CML, heat is concentrated mainly in the upper part of the CML in turbid waters, and the same process takes place there as at the stage of CML formation: first, a region of warmer and denser waters appears, which then 'collapses' due to unstable stratification, leading to mixing; such a process is repeated many times for the entire duration of radiative heating. The radiation flux is more evenly distributed throughout

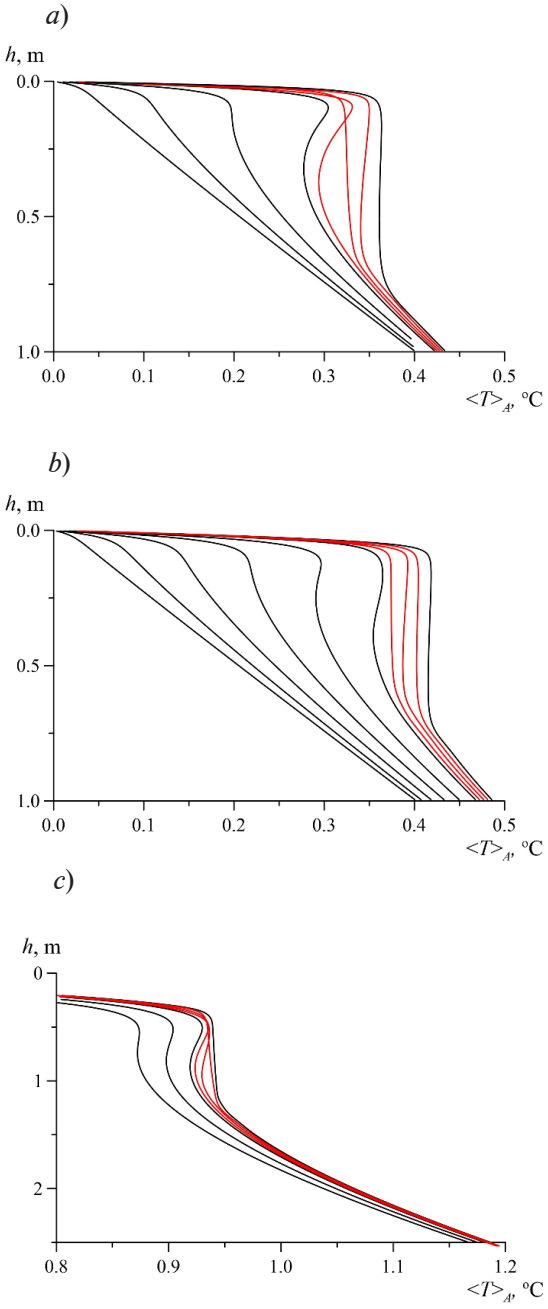

Fig. 4. Time evolution of temperature dependences averaged over horizontal planes on lake depth for V3 (*a*), V1(*b*) and V2 (*c*) Different time periods of temperature measurements with an hour interval (black curves) are shown for the three cases; cases V1 and V3 'started' simultaneously (from the 1st hour) and lasted 6 and 4 hours, respectively (until the 7th and 5th hours); case V2 started from 55th hour and lasted 3 hours. Three additional time points were taken within the last hour segment of each case with a 15-minute interval (red curves) which began at 4 h 15 min (V3), 6 h 15 min (V1) and 57 h 15 min (V2)

the water column in clear waters, warming up the CML more uniformly; the formation of an unstable stratification region in the upper part of the CML occurs much later. As known from field observations, CML often does not often form with a sufficiently high degree of water transparency; the water temperature simply gradually increases at all horizons.

Thus, the distribution of heat to a greater depth along the water column, characteristic of more transparent waters ($\gamma_1 = \gamma_2 = 0.7$ m^{-1}), leads to a faster temperature growth in the upper part of the stratified layer located below the CML, compared with the situation for turbid waters ($\gamma_1 = \gamma_2 = 2.7$ m^{-1}), when the greatest accumulation of energy occurs in the upper layers of the water column, and the lower layers receive virtually no heat. Furthermore, it should be borne in mind that the thickness of the under-ice gradient layer is smaller in more turbid water (see Fig. 5), the temperature gradient in this layer is correspondingly greater, and therefore the heat flux from water to ice is more intense for higher values of the extinction coefficient than in the case of more transparent water (this is confirmed by the graphs of the dependence of average heat flux into the ice given below). The consequence of all these factors is that, for example, on day 4 (see Fig. 5,*b*), the temperature in the stably stratified layer near the lower boundary of the CML for case V2 is significantly higher than for other cases, and the situation is similar in the following days.

As for the position of the lower boundary of the CML, a rather pronounced difference between the cases is observed on the third day from the start of the simulations. The greatest CML depth is observed for V3 ($\gamma_1 = \gamma_2 = 2.7$ m^{-1}), and the smallest depth for V2 ($\gamma_1 = \gamma_2 = 0.7$ m^{-1}). This result was to be expected, since (as noted above) the CML layer for the case V3 was formed earlier than in other cases, and the energy pumped into it serves not only to increase its temperature, but also to deepen the CML. For V2, due to more uniform heating, the incoming energy is spent not only on the formation of CML, but also the increase in temperature in the lower region of stable stratification (see Fig. 5,*a*).

Upon formation of the CML, which occurs at different times from the start of the simulations for different cases (see Fig. 5), the CML continues to deepen at different rates. As seen from Fig. 5, the deepening rate is the highest for V2, the same as the temperature growth rate, which is associated with a stronger penetration of solar radiation into the water column.

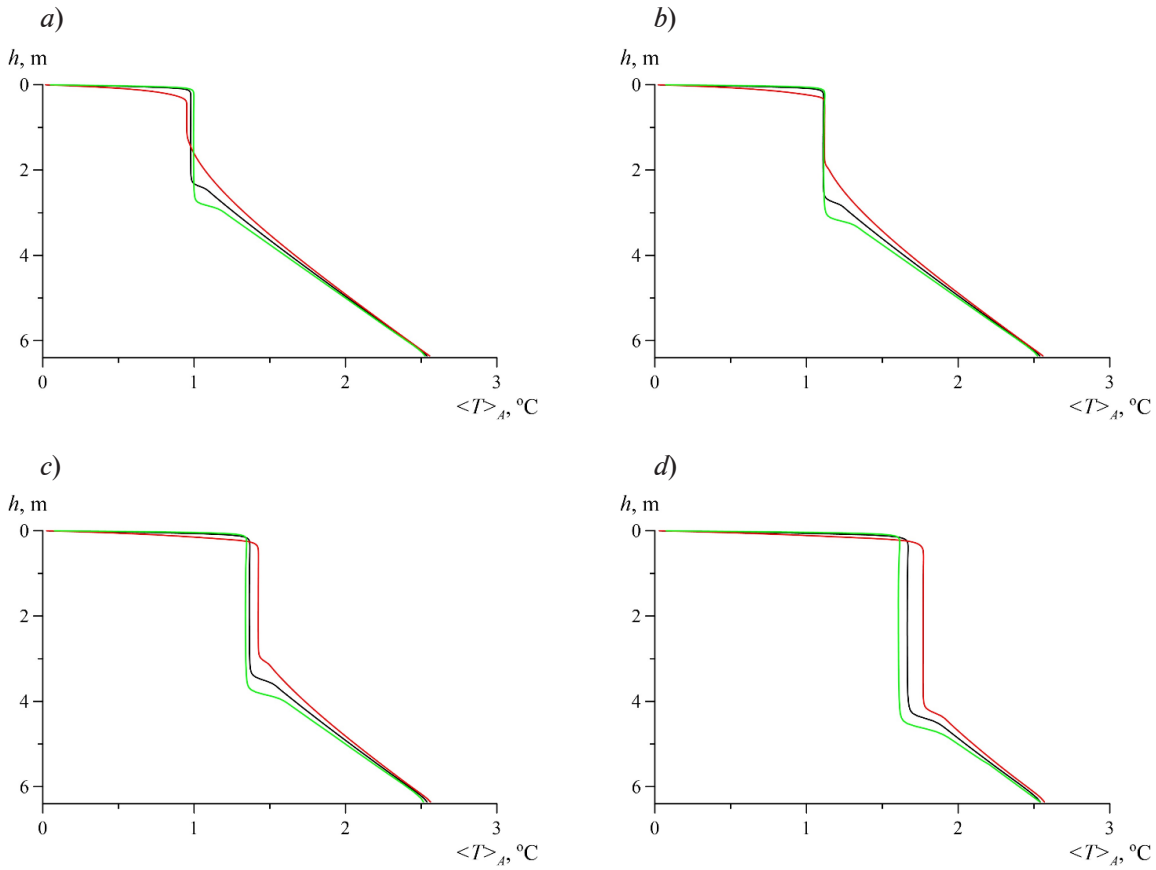

Fig. 5. Comparison of dependences of temperature averaged over horizontal planes on lake depth, obtained at different time points (*a*–*d*) for V1 (black curves), V2 (red) and V3 (green): 16:00 of day 3 (formation of stable CML for V2) (*a*); 15:00 of day 4 (*b*); 15:00 of day 6 (*c*); 15:00 of day 9 (*d*)

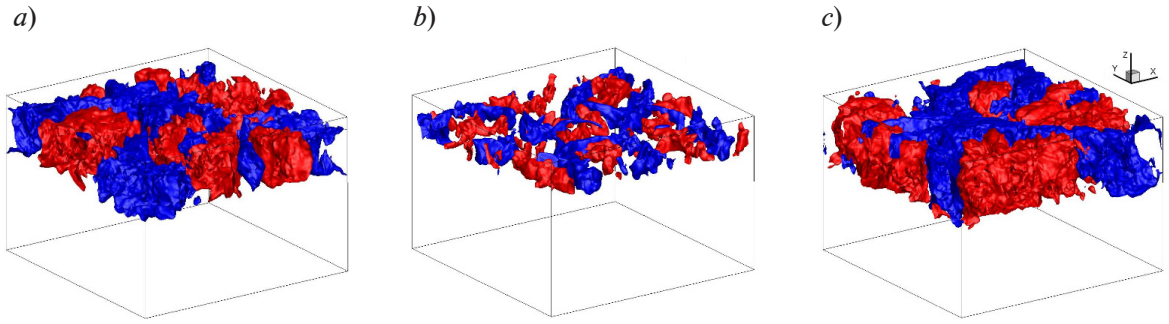

Fig. 6. Isosurfaces of average vertical velocity component V_z ($|<V_z>| = 0.6$ mm/s) for day 4 at 15:00 for cases V1 (a), V2(*b*) and V3 (*c*); averaging period of 1 hour

Additionally, notice the existence of the so-called entrainment layer, a small section of the temperature profile near the lower boundary of the CML, where the temperature increases sharply and then becomes a linear profile in the region of stable stratification. The presence of such a region is also confirmed by field observations [8]. The lower the transparency of the water, the greater the temperature jump observed in the entrainment layer at each point in time; the magnitude of this jump increases over time. The entrainment layer is virtually absent for V2 (with the highest degree of water transparency) in the early days of the CML evolution; it becomes distinguishable in temperature profiles only on the 3rd day from the time of CML formation.

The CML depths for all three cases become close by day 9. To gain a better understanding of the further evolution of CML, it is necessary to conduct simulations at longer time intervals, which is difficult within the problem statement used due to the relatively small size of the computational domain and the coarseness of the computational mesh used near the bottom.

The presence of large-scale vortices filling the entire depth of the CML was observed in previous field and model studies of well-developed RDC [9, 24]. At a certain stage of RDC evolution, the sizes of the vortex structures become commensurate with the depth of the CML, and an increase in the size of the vortex structures can be expected with an increase in the depth of the mixed layer.

Our model calculations indicate the number of large-scale vortex structures in the computational domain is greater at the initial stage of the RDC (with a smaller CML depth) than at subsequent stages, when the depth of the CML increases. Fig. 6 shows the corresponding illustrations as isosurfaces of the vertical velocity component for the 4th day from the start of the simulations. For example, as evident from Fig. 6,*b*, showing the flow structure for V2, if the CML depth is about one meter, the computational domain contains 5–6 vortices whose size in horizontal directions is also about one meter. As seen from Fig. 6, *a*, *c*, showing the results for V1 and V3, the CML depth reaches 2–3 m; the characteristic size of the vortices increases and their number decreases. As RDC develops, the detected characteristic of the evolution of the CML vortex structure imposes certain restrictions on the duration of numerical simulations with the selected size of the computational domain: after a certain period, the size of large-scale structures turns out to be commensurate with the size of the computational domain in horizontal directions, while the influence of periodic boundary conditions can significantly affect the computational accuracy. Therefore, a larger computational domain should be used for longer simulations than in the present study (i.e., over 9 days, with a commensurate level of external energy pumping).

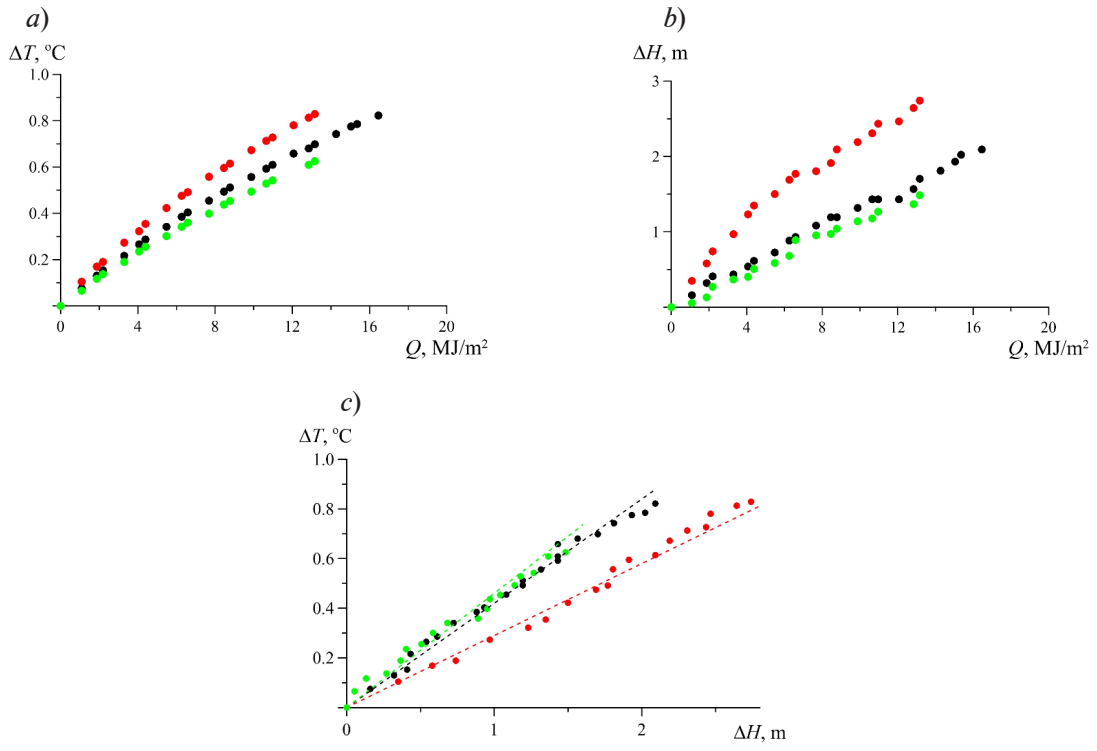

Fig. 7. Increments of CML temperature (*a*) and depth (*b*) as functions of cumulative heat flux; functional relationship between increments of CML temperature and depth (*c*) for cases V1 (black symbols), V2 (red symbols) and V3 (green symbols); dashed lines are linear approximations of function ΔT (ΔH); the results correspond to the period from the 4th day since the start of the process

As for the time evolution of large-scale vortices at different extinction coefficients, it is similar in all three cases. A more detailed analysis of the evolution of vortex structures in CML for the initial case is given in [17].

Let us consider the integral characteristics of CML evolution: the increments of CML depth and temperature as functions of cumulative energy entering the system. The dependences for the increments of CML temperature and depth on the cumulative heat flux (Fig. 7) reflect the above results obtained for the evolution of the temperature profile for different transparencies (see Fig. 5). The highest rates of temperature growth and deepening of the lower CML boundary are observed for case V2 (the clearest waters). Therefore, more uniform energy pumping along the depth leads to higher variation rates of the integral RDC parameters on the days under consideration.

In general, the time dynamics of CML depth (h_{CML}) is determined by the following equation [3, 25]:

$$\frac{dh_{\text{CML}}}{dt} = (1+2A)\frac{B_s}{N^2 h_{\text{CML}}}, \tag{7}$$

where A is the entrainment rate (according to different data, it varies within the range of 0.1–0.3); N is the buoyancy frequency, $N = (\beta g \Gamma)^{0.5}$ (Γ is the temperature gradient in the stratified bottom layer); B_s is the buoyancy flux on the surface, $B_s = \beta g I_s$ (I_s is the kinematic flux, as discussed above).

In the simplest hypothetical case, when the increments in depth h_{CML} and temperature T_{CML} are not accompanied by transformations in the underlying stratified layer [26], $A = 0$ and, accordingly, the heat balance in CML can be written as follows:

$$h_{\text{CML}} \frac{dT_{\text{CML}}}{dt} = I_s. \tag{8}$$

A simple equation directly follows Eqs. (7) and (8), relating the growth rates of CML depth and temperature:

$$\frac{dT_{\text{CML}}}{dh_{\text{CML}}} = \Gamma. \tag{9}$$

In the general case, when $A \neq 0$, Eq. (7) is reduced to the following form after integration:

$$h_{\text{CML}}^2 - h_0^2 = 2(1+2A)\frac{\Delta Q}{\Gamma \rho C_p}, \tag{10}$$

where h_0 is the CML depth at the time of its complete formation.

Table

Computational values of temperature gradient Γ in bottom layer and entrainment rate *A* for three cases

Case	Extinction coefficients, m^{-1}	Γ, °C/m	*A*
V1	$\gamma_1 = 2.7$, $\gamma_2 = 0.7$	0.42	0.17
V2	$\gamma_1 = \gamma_2 = 0.7$	0.29	0.24
V3	$\gamma_1 = \gamma_2 = 2.7$	0.46	0.13

Note. Case V1 corresponds to field observations. Cases V2 and V3 correspond to clear and turbid water, respectively.

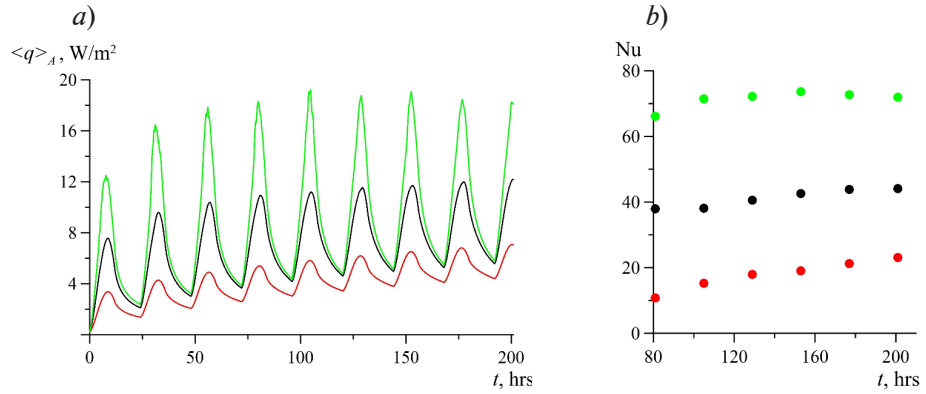

Fig. 8. Time evolution of average heat flux density on the upper wall of the computational domain (*a*) and Nusselt numbers (*b*) calculated for the period from day 4 to day 9 (data collected daily at 15:00) for cases V1 (curve and symbols in black), V2 (red curve and symbols), V3 (green curve and symbols)

The values of Γ (temperature gradient in the stratified bottom layer) and the entrainment rate A obtained in the considered cases are shown in Table.

The values of Γ in cases V1 and V3 are close to each other and to the value of the temperature gradient of 0.4 °C/m set at the lower boundary of the computational domain. A noticeable deviation is observed for V2, apparently induced by the variation in the gradient in the upper part of the stratified layer due to its heating by the radiation flux (see Fig. 5). The value of entrainment rate A increases with an increase in the degree of transparency of the water. The computational results are generally in good agreement with the theory.

Let us now consider the heat fluxes into the ice for different cases (Fig. 8). The Nusselt number is calculated as follows:

$$\mathrm{Nu} = \frac{< q >_A h_{\mathrm{CML}}}{\lambda T_{\mathrm{CML}}}, \tag{11}$$

where $<q>_A$, W/m^2, is the heat flux density on the upper wall of the computational, averaged over the surface.

Fig. 8,*a* shows the dependences of the surface-averaged heat flux into the ice, and Fig. 8,*b* shows the average values of the Nusselt number over the diurnal period. Let us note the characteristic features in the evolution of the heat flux: at the beginning of each day, there is a sharp increase in the heat flux, reaching its maximum between 13:00 and 14:00 (it is assumed that daylight begins at 6 in the morning). After that, there is a decrease in heat flux, so that this decrease is more gradual in the evening and night periods (from 18:00 to 6:00 of the next day) compared to the morning hours. The maxima of heat fluxes during one day, as well as the average values of the Nusselt numbers, first increase day by day, and then reach an almost constant value. Notice the strong sensitivity of heat fluxes and Nusselt numbers to the degree of transparency of water: the less transparent the water, the greater the heat flux into the ice. This in turn means that less heat penetrates the depth of the CML if the water is less transparent. This conclusion is consistent with the results obtained by a study on RDC [27], considering a model problem of convection in a closed cavity under radiatively driven heating and adiabatic walls; it was found that the intensity of heat transfer with CML increases for clearer water.

Let us compare the fluctuation characteristics for three cases, namely, the diagonal components of the Reynolds stress tensor $<V_i^2>$, averaged over both horizontal cross section and time (for 1 hour). Consider the evolution of velocity fluctuations at a depth of 2.5 m (Fig. 9). The evolution of fluctuations is also periodic: during the day, fluctuations increase following an increase in the radiative intensity, and then decrease to almost zero at night. The maximum fluctuations are observed in the time interval from 13 to 14 hours, while the maximum value changes day by day: as the CML forms and its depth increases, the fluctuation maximum first increases, and then begins to oscillate near a certain value. However, starting from about the ninth day, the maximum

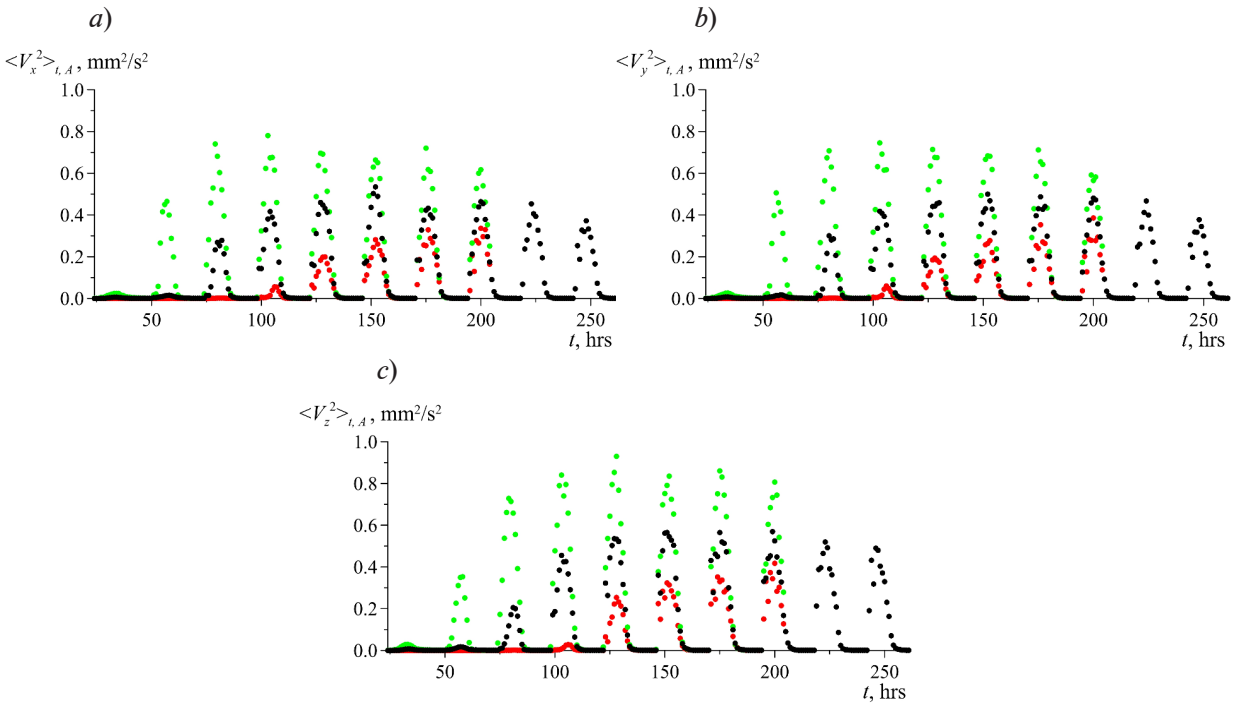

Fig. 9. Time evolution in horizontal (*a*, *b*) and vertical (*c*) velocity fluctuations V_x (*a*), V_y (*b*) and V_z (*c*), averaged over the horizontal plane and over time (averaging period of 1 hour), for cases V1 (black dots), V2 (red dots) and V3 (green dots)
The averaging plane was located at a distance of 2.5 m from the upper boundary of the computational domain

of velocity fluctuations decreases. This may indirectly indicate that large-scale structures are strongly constricted by horizontal periodic boundaries, which leads to the influence of boundary conditions on the flow and suppression of fluctuations in the CML. Note that the level of vertical fluctuations is noticeably higher than the level of horizontal ones for all time points considered. As for the effect of the degree of water transparency, the highest values of $<V_i^2>_{t,A}$ are observed for case V3, and the lowest for V2. Apparently, this is due to the fact that the process of collapse of the temperature profile is less intense in more transparent waters.

Conclusion

The paper reports on numerical simulation of radiatively-driven convection in a model problem simulating real processes occurring in an ice-covered shallow lake exposed to penetrating solar radiation. We considered three cases differing by the degree of water transparency (this degree is expressed by different extinction coefficients γ). The unsteady process of the formation and evolution of a convective mixed layer (CML), starting from a given steady state with a linear temperature profile and zero velocity field, was analyzed for all cases based on implicit large eddy simulation (ILES).

As a result of the simulation, it was found that CML appears the quickest (within about 5 hours) for case V3 (with the highest value of γ, i.e., the lowest degree of water transparency), CML forms slightly later (about 7 hours) in the intermediate (initial) case V1, and a fully developed CML appears only on the third day after the start of the simulations (after about 57 hours) in the case with the highest degree of water transparency, V2. The highest growth rates of CML temperature and depth since its formation are observed for the case V2 (the highest degree of water transparency).

Thus, despite the later formation of CML in the case of clear water (V2), its further evolution occurs somewhat faster than in other cases with lower degrees of transparency.

The simulations were performed for a time period of nine days; the size of the vortex structures in the mixed layer gradually increased and became commensurate with the size of the computational domain in the horizontal directions.

The integral characteristics of the CML were calculated, namely, the increments of CML depth and temperature as functions of the cumulative energy entering the system; the values of the entrainment rate were evaluated as well. It was found that the general dynamics of temperature and depth growth in CML corresponds to theoretical concepts and field observations; the entrainment rate is noticeably higher for the case with the highest degree of water transparency (V2) than for the other two cases.

The time dependences of heat flux into the ice (average over the surface) and Nusselt number (average over the daytime period) were obtained. Analyzing the dependences, we concluded that the maxima of heat fluxes during one day as well as the average values of the Nusselt number first increase day by day, subsequently reaching an almost constant value; a strong sensitivity of heat fluxes and Nusselt numbers to the degree of water transparency is observed: the less clear the water, the higher the heat flux into the ice. This is due to the fact that the depth of the under-ice gradient layer is the smallest in darker waters, and the magnitude of the temperature gradient in this layer is the largest.

The evolution of velocity fluctuations is also considered, also appearing to be periodic: during the day, the fluctuations increase following an increase in the intensity of solar radiation, then decreasing to almost zero at night. As the CML forms and its depth increases, the maximum of diurnal fluctuations first increases, and then begins to oscillate near a certain value. Starting from about the 9th day, the maximum of velocity fluctuations begins to decrease, suggesting a noticeable effect of boundary conditions on the flow leading to suppression of fluctuations in the CML. Calculations also showed that the higher the degree of transparency of the water, the lower the values of velocity fluctuations. This is due to a less intense process of temperature profile collapse in the upper part of the CML.

Thus, the conducted study allowed to obtain new information about the effect of water transparency on the formation and development of CML during radiative heating of ice-covered lakes.

As a further direction of research, we intend to consider longer time periods, using a larger computational domain, since boundary conditions begin to affect flows, which leads to suppression of fluctuations in the CML layer and may also affect the convective characteristics.

The results were obtained using the resources of the Supercomputer Center at Peter the Great St. Petersburg Polytechnic University (www.spbstu.ru).

REFERENCES

1. **Farmer D. M.,** Penetrative convection in the absence of mean shear, Q. J. R. Meteorol. Soc. 101 (430) (1975) 869–891.

2. **Jonas T., Terzhevik A. Y., Mironov D. V., Wüest A.,** Radiatively driven convection in an ice-covered lake investigated by using temperature microstructure technique, J. Geophys. Res. 08 (6) (2003) 3183.

3. **Bouffard D., Wüest A.,** Convection in lakes, Annu. Rev. Fluid Mech. 51 (1) (2019) 189–215.

4. **Kelley D.,** Convection in ice-covered lakes: effects on algal suspension, J. Plankton Res. 19 (12) (1997) 1859–1880.

5. **Kiili M., Pulkkanen M., Salonen K.,** Distribution and development of under-ice phytoplankton in 90-m deep water column of Lake Päijänne (Finland) during spring convection, Aquat. Ecol. 43 (3) (2009) 707–713.

6. **Huang W., Zhang Z., Li Z., et al.,** Under-ice dissolved oxygen and metabolism dynamics in a shallow lake: The critical role of ice and snow, Water Resour. Res. 57 (5) (2021) e2020WR027990.

7. **Mironov D., Terzhevik A., Kirillin G., et al.,** Radiatively driven convection in ice-covered lakes: Observations, scaling, and a mixed layer model, J. Geophys. Res. 107 (C4) (2002) 3032.

8. **Mironov D. V., Terzhevik A. Yu.,** Spring convection in ice-covered freshwater lakes, Izv. – Atmos. Ocean. Phys. 36 (5) (2000) 627–634.

9. **Mironov D. V., Danilov S. D., Olbers D. J.** Large-eddy simulation of radiatively-driven convection in ice covered lakes, In book: Casamitjana X (Ed.), Proc. Sixth Workshop Phys. Proces. Nat. Waters. June 27–29, 2001; Girona, Catalonia, Spain (2001) 71–75.

10. **Santo M. A., Toffolon M., Zanier G., et al.,** Large eddy simulation (LES) of wind-driven circulation in a peri-alpine lake: Detection of turbulent structures and implications of a complex surrounding orography, J. Geophys. Res. Oceans. 122 (6) (2017) 4704–4722.

11. **Zhang Y., Huang Q., Ma Y., et al.,** Large Eddy Simulation of boundary-layer turbulence over the heterogeneous surface in the source region of the Yellow River, Atmos. Chem. Phys. 21 (20) (2021) 15949–15968.

12. **Silano G., Sreenivasan K. R., Verzicco R.,** Numerical simulations of Rayleigh–Bénard convection for Prandtl numbers between 10^{-1} and 10^{4} and Rayleigh numbers between 10^{5} and 10^{9}, J. Fluid Mech. 662 (10 Nov) (2010) 409–446.

13. **Smirnov S. I., Smirnov E. M., Smirnovsky A. A.,** Endwall heat transfer effects on the turbulent mercury convection in a rotating cylinder, St. Petersburg State Polytechnical University Journal. Physics and Mathematics. 10 (1) (2017) 31–46 (in Russian).

14. **Yigit S., Hasslberger J., Klein M.,** Assessment of numerical dissipation in Implicit LES of turbulent Rayleigh–Bénard Convection, In book: García-Villalba M., Kuerten H., Salvetti M. (Eds), Direct and Large Eddy Simulation XII (DLES 2019). Conf. Proc., Book Ser. ERCOFTAC (ERCO, Vol 27), Springer, Cham. (2020) 263–269.

15. **Smirnov S., Smirnovsky A., Zdorovennova G., et al.,** Water temperature evolution driven by solar radiation in an ice-covered lake: A numerical study and observational data, Water. 14 (24) (2022) 4078.

16. **Smirnovsky A. A., Smirnov S. I., Bogdanov S. R., et al.,** Numerical simulation of turbulent mixing in a shallow lake for periods of under-ice convection, Water Resources. 50 (5) (2023) 622–632 (in Russian).

17. **Smirnov S., Smirnovsky A., Zdorovennova G., et al.,** Numerical simulation of radiatively driven convection in a small ice-covered lake with a lateral pressure gradient, Water. 15 (22) (2023) 3953.

18. **Heiskanen J., Mammarella I., Ojala A., et al.,** Effects of water clarity on lake stratification and lake-atmosphere heat exchange, J. Geophys. Res. Atmos. 120 (15) (2015) 7412–7428.

19. **Zhang Q., Ma X.,** How does lake water clarity affect lake thermal processes? Heliyon. 8 (8) (2022) e10359.

20. **Wang M., Wen L., Li Z., et al.,** Mechanisms and effects of under-ice warming water in Ngoring Lake of Qinghai–Tibet Plateau, Cryosphere. 16 (9) (2022) 3635–3648.

21. **Petrov M. P., Terzhevik A. Yu., Zdorovennov R. E., Zdorovennova G. E.,** The thermal structure of a shallow lake in early winter, Water Resources. 33 (2) (2006) 154–162 (in Russian).

22. **Smirnov E. M., Zaytsev D. K.,** Finite volume method as applied to hydro-and gas dynamics and heat transfer problems in complex geometry domains, Nauchno-tekhnicheskiye vedomosti (SPbGTU) [Scientific and Technical Journal (SPbGTU)]. (2 (36) (2004) 70–81.

23. **Smirnov E. M., Zaitsev D. K., Smirnovsky A. A., et al.,** Assessment of several advanced numerical algorithms implemented in the CFD Code SINF/Flag-S for supercomputer simulations, Supercomput. Front. Innov. 11 (2) (2024) 14–31.

24. **Bogdanov S., Zdorovennova G., Volkov S., et al.,** Structure and dynamics of convective mixing in Lake Onego under ice-covered conditions, Inland Waters. 9 (2) (2019) 177–192.

25. **Zilitinkevich S. S.,** Turbulent penetrative convection, Edit. by B. Henderson-Sellers, Avebury Technical, Aldershot, UK, 1991.

26. **Carson D. J., Smith F. B.,** Thermodynamic model for the development of a convectively unstable boundary layer, In book: F. N. Frenkiel, R.E. Munn (Eds). Turbulent diffusion in environmental pollution. Book series "Advances in Geophysics". Vol. 18. Part. A. Proc. Sympos. at Charlottesville, 8–14 April 1973, Virginia, USA, Academic Press (Elsevier), New York (1975) 111–124.

27. **Bouillaut V., Lepot S., Aumaotre S., Gallet B.,** Transition to the ultimate regime in a radiatively driven convection experiment, J. Fluid Mech. 861 (25 Febr) (2019) R5.

СПИСОК ЛИТЕРАТУРЫ

1. **Farmer D. M.** Penetrative convection in the absence of mean shear // Quarterly Journal of the Royal Meteorological Society. 1975. Vol. 101. No. 430. Pp. 869–891.

2. **Jonas T., Terzhevik A. Y., Mironov D. V., Wüest A.** Radiatively driven convection in an ice-covered lake investigated by using temperature microstructure technique // Journal of Geophysical Research. 2003. Vol. 108. No. 6. P. 3183.

3. **Bouffard D., Wüest A.** Convection in lakes // Annual Review of Fluid Mechanics. 2019. Vol. 51. No. 1. Pp. 189–215.

4. **Kelley D.** Convection in ice-covered lakes: effects on algal suspension // Journal of Plankton Research. 1997. Vol. 19. No. 12. Pp. 1859–1880.

5. **Kiili M., Pulkkanen M., Salonen K.** Distribution and development of under-ice phytoplankton in 90-m deep water column of Lake Päijänne (Finland) during spring convection // Aquatic Ecology. 2009. Vol. 43. No. 3. Pp. 707–713.

6. **Huang W., Zhang Z., Li Z., Leppäranta M., Arvola L., Song S., Huotari J., Lin Z.** Under-ice dissolved oxygen and metabolism dynamics in a shallow lake: The critical role of ice and snow // Water Resources Research. 2021. Vol. 57. No. 5. P. e2020WR027990.

7. **Mironov D., Terzhevik A., Kirillin G., Jonas T., Malm J., Farmer D.** Radiatively driven convection in ice-covered lakes: Observations, scaling, and a mixed layer model // Journal of Geophysical Research. 2002. Vol. 107. No. C4. P. 3032.

8. **Mironov D. V., Terzhevik A. Yu.** Spring convection in ice-covered freshwater lakes // Izvestiya, Atmospheric and Oceanic Physics. 2000. Vol. 36. No. 5. Pp. 627–634.

9. **Mironov D. V., Danilov S. D., Olbers D. J.** Large-eddy simulation of radiatively-driven convection in ice covered lakes // Casamitjana X. (Ed.) Proceedings of the Sixth Workshop on Physical Processes in Natural Waters. June 27–29, 2001; Girona, Catalonia, Spain. 2001. Pp. 71–75.

10. **Santo M. A., Toffolon M., Zanier G., Giovannini L., Armenio V.** Large eddy simulation (LES) of wind-driven circulation in a peri-alpine lake: Detection of turbulent structures and implications of a complex surrounding orography // Journal of Geophysical Research: Oceans. 2017. Vol. 122. No. 6. Pp. 4704–4722.

11. **Zhang Y., Huang Q., Ma Y., Luo J., Wang C., Li Z., Chou Y.** Large eddy simulation of boundary-layer turbulence over the heterogeneous surface in the source region of the Yellow River // Atmospheric Chemistry and Physics. 2021. Vol. 21. No. 20. Pp. 15949–15968.

12. **Silano G., Sreenivasan K. R., Verzicco R.** Numerical simulations of Rayleigh–Bénard convection for Prandtl numbers between 10^{-1} and 10^{4} and Rayleigh numbers between 10^{5} and 10^{9} // Journal of Fluid Mechanics. 2010. Vol. 662. 10 November. Pp. 409–446.

13. **Смирнов С. И., Смирнов Е. М., Смирновский А. А**. Влияние теплопереноса в торцевых стенках на турбулентную конвекцию ртути во вращающемся цилиндре // Научно-технические ведомости СПбПУ. Физико-математические науки. 2017. Т. 10. № 1. С. 31–46.

14. **Yigit S., Hasslberger J., Klein M.** Assessment of numerical dissipation in Implicit LES of turbulent Rayleigh–Bénard convection // García-Villalba M., Kuerten H., Salvetti M. (Eds). Direct and Large Eddy Simulation XII (DLES 2019). Conference Proceedings. Book series: ERCOFTAC (ERCO, Vol 27). Switzerland: Springer, Cham. 2020. Pp. 263–269.

15. **Smirnov S., Smirnovsky A., Zdorovennova G., Zdorovennov R., Palshin N., Novikova I., Terzhevik A., Bogdanov S.** Water temperature evolution driven by solar radiation in an ice-covered lake: A numerical study and observational data // Water. 2022. Vol. 14. No. 24. P. 4078.

16. **Смирновский А. А., Смирнов С. И., Богданов С. Р., Здоровеннов Р. Э., Здоровеннова Г. Э.** Численное моделирование турбулентного перемешивания в мелководном озере для периодов подледной конвекции // Водные ресурсы. 2023. Т. 50. № 5. С. 622–632.

17. **Smirnov S., Smirnovsky A., Zdorovennova G., Zdorovennov R., Efremova T., Palshin N., Bogdanov S.** Numerical simulation of radiatively driven convection in a small ice-covered lake with a lateral pressure gradient // Water. 2023. Vol. 15. No. 22. P. 3953.

18. **Heiskanen J., Mammarella I., Ojala A., et al.** Effects of water clarity on lake stratification and lake-atmosphere heat exchange // Journal of Geophysical Research: Atmospheres. 2015. Vol. 120. No. 15. Pp. 7412–7428.

19. **Zhang Q., Ma X.** How does lake water clarity affect lake thermal processes? // Heliyon. 2022. Vol. 8. No. 8. P. e10359.

20. **Wang M., Wen L., Li Z., Leppäranta M., Stepanenko V., Zhao Y., Niu R., Yang L., Kirillin G.** Mechanisms and effects of under-ice warming water in Ngoring lake of Qinghai–Tibet Plateau // The Cryosphere. 2022. Vol. 16. No. 9. Pp. 3635–3648.

21. **Петров М. П., Тержевик А. Ю., Здоровеннов Р. Э., Здоровеннова Г. Э.** Особенности термической структуры мелководного озера в начале зимы // Водные ресурсы. 2006. Т. 33. № 2. С. 154–162.

22. **Смирнов Е. М., Зайцев Д. К.** Метод конечных объемов в приложении к задачам гидрогазодинамики и теплообмена в областях сложной геометрии // Научно-технические ведомости СПбГТУ. 2004. № 2 (36). С. 70–81.

23. **Smirnov E. M., Zaitsev D. K., Smirnovsky A. A., Kolesnik E. V., Pozhilov A. A.** Assessment of several advanced numerical algorithms implemented in the CFD Code SINF/Flag-S for supercomputer simulations // Supercomputing Frontiers and Innovations. 2024. Vol. 11. No. 2. Pp. 14–31.

24**. Bogdanov S., Zdorovennova G., Volkov S., Zdorovennov R., Palshin N., Efremova T., Terzhevik A., Bouffard D.** Structure and dynamics of convective mixing in Lake Onego under ice-covered conditions // Inland Waters. 2019. Vol. 9. No. 2. Pp. 177–192.

25. **Зилитинкевич С. С.** Проникающая турбулентная конвекция. Таллин: Валгус, 1989. 210 с.

26. **Carson D. J., Smith F. B.** Thermodynamic model for the development of a convectively unstable boundary layer // F. N. Frenkiel, R.E. Munn (Eds). Turbulent diffusion in environmental pollution. Book series “Advances in Geophysics”. Vol. 18. Part. A. Proceedings of a Symposium held at Charlottesville. 8–14 April 1973, Virginia, USA. New York; Academic Press (Elsevier), 1975. Pp. 111–124.

27. **Bouillaut V., Lepot S., Aumaotre S., Gallet B.** Transition to the ultimate regime in a radiatively driven convection experiment // Journal of Fluid Mechanics. 2019. Vol. 861. 25 February. P. R5.

THE AUTHORS

SMIRNOV Sergei I.
Northern Water Problems Institute of Karelian Research Centre of RAS
11 Pushkinskaya St., Petrozavodsk, 185000, Russia
sergeysmirnov92@mail.ru
ORCID: 0000-0002-3972-9259

SMIRNOVSKY Alexander A.
Peter the Great St. Petersburg Polytechnic University
29 Politechnicheskaya St., St. Petersburg, 195251, Russia
smirta@mail.ru
ORCID: 0000-0001-7608-7120

BOGDANOV Sergey R.
Northern Water Problems Institute of Karelian Research Centre of RAS
11 Pushkinskaya St., Petrozavodsk, 185000, Russia
sergey.r.bogdanov@mail.ru
ORCID: 0000-0003-4150-2712

ZDOROVENNOVA Galina E.
Northern Water Problems Institute of Karelian Research Centre of RAS
11 Pushkinskaya St., Petrozavodsk, 185000, Russia
zdorovennova@gmail.com
ORCID: 0000-0003-2726-0104

EFREMOVA Tatiana V.
Northern Water Problems Institute of Karelian Research Centre of RAS 11 Pushkinskaya St., Petrozavodsk, 185000, Russia
efremova@nwpi.krc.karelia.ru
ORCID: 0000-0003-0313-6731

PALSHIN Nikolay I.
Northern Water Problems Institute of Karelian Research Centre of RAS
11 Pushkinskaya St., Petrozavodsk, 185000, Russia
npalshin@mail.ru
ORCID: 0000-0003-1540-3788

ZDOROVENNOV Roman E.
Northern Water Problems Institute of Karelian Research Centre of RAS
11 Pushkinskaya St., Petrozavodsk, 185000, Russia
romga74@gmail.com
ORCID: 0000-0003-1695-4872

СВЕДЕНИЯ ОБ АВТОРАХ

СМИРНОВ Сергей Игоревич – *кандидат физико-математических наук, старший научный сотрудник лаборатории гидрофизики Института водных проблем Севера Карельского научного центра РАН.*
185000, Россия, Республика Карелия, г. Петрозаводск, Пушкинская ул., 11
sergeysmirnov92@mail.ru
ORCID: 0000-0002-3972-9259

СМИРНОВСКИЙ Александр Андреевич – *кандидат физико-математических наук, доцент Высшей школы прикладной математики и вычислительной физики Санкт-Петербургского политехнического университета Петра Великого.*
195251, Россия, г. Санкт-Петербург, Политехническая ул., 29
smirta@mail.ru
ORCID: 0000-0001-7608-7120

БОГДАНОВ Сергей Рэмович – *доктор физико-математических наук, ведущий научный сотрудник лаборатории гидрофизики Института водных проблем Севера Карельского научного центра РАН.*
185000, Россия, Республика Карелия, г. Петрозаводск, Пушкинская ул., 11
sergey.r.bogdanov@mail.ru
ORCID: 0000-0003-4150-2712

ЗДОРОВЕННОВА Галина Эдуардовна – *кандидат географических наук, ведущий научный сотрудник лаборатории гидрофизики Института водных проблем Севера Карельского научного центра РАН.*
185000, Россия, Республика Карелия, г. Петрозаводск, Пушкинская ул., 11
zdorovennova@gmail.com
ORCID: 0000-0003-2726-0104

ЕФРЕМОВА Татьяна Владимировна – *кандидат географических наук, старший научный сотрудник лаборатории гидрофизики Института водных проблем Севера Карельского научного центра РАН.*
185000, Россия, Республика Карелия, г. Петрозаводск, Пушкинская ул., 11
efremova@nwpi.krc.karelia.ru
ORCID: 0000-0003-0313-6731

ПАЛЬШИН Николай Иннокентьевич – *кандидат географических наук, старший научный сотрудник лаборатории гидрофизики Института водных проблем Севера Карельского научного центра РАН.*
185000, Россия, Республика Карелия, г. Петрозаводск, Пушкинская ул., 11
npalshin@mail.ru
ORCID: 0000-0003-1540-3788

ЗДОРОВЕННОВ Роман Эдуардович – *кандидат географических наук, старший научный сотрудник лаборатории гидрофизики Института водных проблем Севера Карельского научного центра РАН.*
185000, Россия, Республика Карелия, г. Петрозаводск, Пушкинская ул., 11
romga74@gmail.com
ORCID: 0000-0003-1695-4872

Received 19.10.2024. Approved after reviewing 26.11.2024. Accepted 26.11.2024.
Статья поступила в редакцию 19.10.2024. Одобрена после рецензирования 26.11.2024. Принята 26.11.2024.